https://doi.org/10.5194/egusphere-2026-1929
Preprint. Discussion started: 28 April 2026

Monitoring Land Subsidence at San Francisco International Airport Using Satellite Radar Interferometry

Oluwaseyi Dasho[1,2] and Manoochehr Shirzaei[1,2]
[1]Department of Geosciences, Virginia Tech, Blacksburg, USA.
[2]Institute for Water, Environment and Health, United Nations University, Richmond Hill, Ontario, Canada.

Corresponding author: Oluwaseyi Dasho (seyidasho@vt.edu)

https://doi.org/10.5194/egusphere-2026-1929
Preprint. Discussion started: 28 April 2026

Abstract:

Coastal airports are increasingly vulnerable to infrastructure degradation from land subsidence exacerbated by sea-level rise (SLR) and extreme weather events. San Francisco International Airport (SFO), situated on a reclaimed land overlying thick compressible Young Bay Mud, provides a representative case study for understanding the implications of land subsidence on infrastructure resilience. This study employs advanced Interferometric Synthetic Aperture Radar (InSAR) techniques to measure and analyze spatially detailed subsidence at SFO from 2017 to 2024. We integrate the InSAR data with subsurface stratigraphy derived from geotechnical investigations and historical construction records to identify and quantify patterns and drivers of subsidence. The results indicate spatially heterogeneous subsidence rates, with rates exceeding −10.0 ± 0.1 mm/yr, concentrated primarily under the airfield's infrastructure, notably along Runway 10R/28L. Temporal analyses of deformation time series reveal significant variability and nonlinear trends, likely due to seasonal groundwater fluctuations, construction activities, and heterogeneous subsurface stratigraphy. Areas with older hydraulically placed fills demonstrate higher rates of long-term compaction, emphasizing the critical role of historical construction practices and sediment properties. This study's findings underscore the urgent need for comprehensive and continuous ground deformation monitoring at coastal airports. The implications for infrastructure resilience planning at SFO serve as a valuable model for other coastal airports facing similar geotechnical and climatic challenges.

Keywords: Vertical Land Motion, Subsidence, InSAR, Infrastructure Resilience, Sea-Level Rise, San Francisco International Airport, Coastal Airports.

https://doi.org/10.5194/egusphere-2026-1929
Preprint. Discussion started: 28 April 2026

1 Introduction

Coastal airports, over a thousand of which are situated within the Low-Elevation Coastal Zone (LECZ) globally, are increasingly exposed to compound hazards driven by land subsidence, sea-level rise, and extreme weather events (De Vivo et al., 2022; Griggs, 2020; Yesudian and Dawson, 2021). These processes interact to amplify flood risk, reduce the effectiveness of coastal defenses, and threaten the long-term operability of critical transport infrastructure. Among these hazards, land subsidence, represents a subtle yet significant driver of infrastructure vulnerability (Dasho and Shirzaei, 2025; Nicholls et al., 2021; Shirzaei et al., 2020). Subsidence reduces freeboard for flood defenses, compromises stormwater management systems, exacerbates relative sea-level rise (RSLR) exposure, and creates localized hazards such as pavement cracking and ponding, directly impacting operational safety and maintenance requirements.

San Francisco International Airport (SFO) exemplifies the challenges faced by coastal airports constructed in subsidence-prone regions. The airport was developed primarily through large-scale land reclamation projects that transformed tidal marshes and mudflats into operational airfield space. As a result, much of its infrastructure, including runways, taxiways, and terminal facilities, is founded on thick, highly compressible deposits of Young Bay Mud overlain by hydraulically placed fill materials (Baldwin et al., 2018; Fugro, 2013).

Extensive historical land reclamation, beginning in the early twentieth century and accelerating after World War II, enabled the expansion of SFO into former tidal marshes, mudflats, and shallow bay environments (Fugro, 2013). Early construction practices predated the adoption of modern ground improvement methods such as preloading, surcharging, or deep foundation systems, leaving large portions of the airfield supported by unconsolidated fill and compressible subsoils. The resulting heterogeneity in fill thickness, compaction, and consolidation history has led to spatially variable settlement rates across the airport. Shoreline protection structures, including levees and revetments, provide the first line of defense against tidal inundation; however, these aging systems were not originally designed to accommodate accelerated sea-level rise or continuing subsidence, leading to declining freeboard and increasing flood risk.

The impacts of ongoing subsidence at SFO are well-documented (Stock et al., 2019). Persistent ground deformation has been linked to drainage inefficiencies, localized ponding, and accelerated pavement deterioration, as surface cracking and uneven settlement challenge airport operations. Several studies and engineering reports have highlighted the heightened exposure of SFO to high-tide flooding and storm surge events, especially as effective freeboard margins diminish due to ongoing settlement and rising sea levels (Johnson et al., 2018; Moffatt & Nichol, 2015). These historical and contemporary observations underscore the critical need for comprehensive, continuous ground motion monitoring to inform adaptive infrastructure management and long-term resilience planning.

https://doi.org/10.5194/egusphere-2026-1929
Preprint. Discussion started: 28 April 2026

Satellite-based Interferometric Synthetic Aperture Radar (InSAR) techniques represent a transformative advance for monitoring Vertical Land Motion (VLM) and ensuring infrastructure resilience at large, operationally critical sites like SFO (Bianchini Ciampoli et al., 2020; Gagliardi et al., 2021). Compared to traditional leveling or ground-based surveys, InSAR offers non-invasive, cost-effective, and millimeter-precision measurement capabilities over extensive areas without disrupting airport operations (Shirzaei et al., 2020). This technology enables early detection of localized settlement patterns, quantification of differential motion across complex facilities, and improved forecasting of areas at risk for surface cracking, drainage failure, or flood exposure. The innovation of satellite-based monitoring lies not only in its precision and efficiency but also in its ability to generate actionable data to guide maintenance prioritization, engineering design adjustments, and climate adaptation strategies.

In this study, we integrate InSAR observations to map land subsidence across SFO from 2017 to 2024. The VLM measurements are combined with stratigraphic models derived from geotechnic investigation and historical construction records to elucidate the underlying geotechnical processes driving deformation. We quantify the spatial distribution of subsidence, analyze temporal trends at representative hotspots, investigate the influence of subsurface stratigraphy, and evaluate the relative contributions of historical land reclamation practices, paleoenvironmental setting, and operational aircraft loading. The results provide new insights into the mechanisms governing ongoing ground deformation at SFO and offer a transferable framework for incorporating remote sensing data into infrastructure resilience planning at coastal airports worldwide.

2 Material and Method

2.1 InSAR Analysis

We measured ground deformation at SFO using multitemporal InSAR analysis from Sentinel-1 A/B satellites. The dataset comprises 184 ascending orbit images acquired from February 24, 2017, to May 12, 2024, and 229 descending orbit images acquired from November 13, 2015, to April 23, 2024. From these images, we generated 780 interferograms for ascending mode (heading angle = -13.28°) and 973 interferograms for descending mode (heading angle = 193.29°). Maximum temporal and perpendicular baselines for the dataset were 600 days and 35 m, respectively.

To ensure appropriate spatial resolution, we applied multi-looking factors of 6 (range) by 1 (azimuth), resulting in a pixel size of approximately 15 × 15 meters. Sets of interferometric triplets, consisting of interferograms with diverse temporal baselines, were created using Delaunay Triangulation and dyadic down-sampling methods to minimize phase closure errors (Lee and Shirzaei, 2023). Topographic and flat-earth effects were corrected using the 30-meter resolution Shuttle Radar Topography Mission (SRTM) Digital Elevation Model (Farr et al., 2007) and precise satellite orbital information (Franceschetti and Lanari, 1999). Absolute phase changes were estimated by applying a two-dimensional minimum cost-flow algorithm (Mario Costantini, 1998) to a sparse set of high-quality pixels (Costantini and Rosen, 1999). Line-of-sight (LOS)

https://doi.org/10.5194/egusphere-2026-1929
Preprint. Discussion started: 28 April 2026

displacement time series were computed by integrating unwrapped phase values of the interferograms through a reweighted least-squares approach (Shirzaei, 2013). Atmospheric delays were identified and mitigated using two-dimensional smoothing splines (Lee and Shirzaei, 2023) and wavelet-based filters (Shirzaei and Bürgmann, 2012). Mean LOS displacement rates were derived from the slopes of best-fitting lines applied to each pixel's displacement time series. Final displacement LOS velocities and standard deviations for both ascending and descending datasets are shown in Fig. S1 – S2 of Supporting Information. The standard deviation is derived from the regression uncertainty of the velocity estimate.

The observed LOS displacement velocities represent combined horizontal (east-west, north-south) and vertical (uplift-subsidence) components. Given the polar orbit of Sentinel-1 satellites, only east-west and vertical displacement components could be reliably quantified, thus we assumed negligible north-south motion. Consequently, we combined ascending and descending LOS displacement velocities using co-located pixels to derive accurate, east-west (E) and vertical (U) velocity maps, following the methodology outlined in (Miller and Shirzaei, 2019). The model to combine ascending and descending LOS displacement velocities is represented by Equation 1.

$$\begin{bmatrix} ASC_{LOS} \\ DES_{LOS} \end{bmatrix} = \begin{bmatrix} v_E^{ASC} & v_U^{ASC} \\ v_E^{DES} & v_U^{DES} \end{bmatrix} \begin{bmatrix} E \\ U \end{bmatrix} \quad (1)$$

where, ASC_{LOS} and DES_{LOS} are the ascending and descending Sentinel-1 LOS displacement velocities, respectively. v is the unit vector projecting the displacement onto the LOS (Hanssen, 2001), which are functions of the incidence and heading angles. The final solution to Equation 1 is given by Equation 2:

$$X = A^{-1}L \quad (2)$$

where,

$$X = \begin{bmatrix} E \\ U \end{bmatrix}, A = \begin{bmatrix} v_E^{ASC} & v_U^{ASC} \\ v_E^{DES} & v_U^{DES} \end{bmatrix}, L = \begin{bmatrix} ASC_{LOS} \\ DES_{LOS} \end{bmatrix}$$

The East-west velocity as well as its standard deviation is presented in Fig. S3. Also, the 1σ standard deviation of the VLM is shown in Fig. S4.

The VLM measurement was tie to the IGS14 reference frame using the nearest GNSS station (HSIB) from data provided by the Nevada Geodetic Laboratory.

2.2 Statistical Analysis

https://doi.org/10.5194/egusphere-2026-1929
Preprint. Discussion started: 28 April 2026

We applied the Geographical Detectors (GD) statistical analysis to measure the driving influence of construction year, paleoenvironment and touchdown zone on VLM along the four runways in SFO. The analysis is a spatial statistical technique designed to analyze spatial stratified heterogeneity and identify driving factors behind observed geographical patterns. The method operates on the principle that if an independent variable (X) significantly influences a dependent variable (Y), their spatial distributions should exhibit similarity (Chen et al., 2020; Zhang et al., 2022)

Factor Detector, a component of GD, quantifies the explanatory power of independent variables using the q-statistic:

$$q = 1 - \frac{SSW}{SST}$$

where:

- $SSW = \sum_{h=1}^{L} N_h \sigma_h^2$ (Within sum of squares)
- $SST = N\sigma^2$ (Total sum of squares)
- L = number of strata, N_h = units in stratum h, σ_h^2 = stratum variance

2.3 Ancillary Data

The construction year, paleoenvironment and stratigraphy datasets were extracted from (Fugro, 2013). Reclaimed land area filled in the year 1973 and 1974 were combined and presented as filled in the year 1974.

The stratigraphy dataset reveals multiply subsurface layers which consist of artificial fill, young bay mud, alluvium, and old bay mud. The artificial fill unit comprises very loose to medium-dense, poorly graded sand interspersed with silt, clay, and gravel (Baldwin et al., 2018; Fugro, 2013). Beneath the fill, the young bay mud forms a laterally extensive, highly compressible unit composed of unconsolidated organic-rich clay to silty clay, with thicknesses ranging between 20 to 70 feet across the airport (Baldwin et al., 2018; Fugro, 2013).

The old bay mud, comprising dense to very dense sand and silty sand and stiff to very stiff clay, is generally more consolidated than the overlying young bay mud (Baldwin et al., 2018; Fugro, 2013). Interspersed within the older bay mud sequences are discrete coarse-grained lenses, primarily composed of sand and gravel. Overlying the old bay mud and interbedded with both bay mud units is the Holocene alluvium, consisting of interlayered sand, silt, and clay (Baldwin et al., 2018; Fugro, 2013). At greater depth, the Pleistocene alluvium forms the basal unit, consisting of moderately dense clay, silt, and sand with gravel (Fugro, 2013). This relatively competent stratum marks the approximate boundary below which significant deformation is not expected and thus defines the effective mechanical basement of the profile.

https://doi.org/10.5194/egusphere-2026-1929
Preprint. Discussion started: 28 April 2026

3 Results

3.1 Spatially dense distribution of VLM at SFO

Figure 1a presents the spatial distribution of VLM across SFO, with runway alignments overlaid for reference. The VLM estimates are referenced to the International GNSS Service (IGS14) terrestrial reference frame and span the period from 2017 to 2024. VLM rates exceeding −7 mm/yr are observed indicating intense ground deformation, consistent with previous findings showing similar subsidence rates in portions of the San Francisco Bay Area (Blackwell et al., 2020; Dasho and Shirzaei, 2025; Govorcin et al., 2025). The figure reveals a striking spatial correlation between subsidence rates and the airfield's infrastructure layout. The runway system is delineated by the subsidence pattern, with the highest rates of VLM concentrated directly beneath and adjacent to the runways. The most pronounced deformation is observed along the Runway 10R/28L, particularly near its 10R end, where the subsidence rate reaches −7.8 ± 0.1 mm/yr. Runway 10L/28R exhibits a median subsidence of approximately −5.5 ± 0.1 mm/yr, with maximum rates concentrated in the central section intersecting the crosswind runways. The 1L/19R and 1R/19L runways, display spatially variable subsidence ranging from −2.0 to −7.0 ± 0.1 mm/yr, with the pronounced deformation again occurring at intersections with the other runways. The central intersection zone, where all four runways converge, shows marked differential motion, with localized deformation gradients reaching up to 5 mm/yr over short distances. These sharp spatial variations likely reflect heterogeneous subgrade conditions and non-uniform loading across the pavement structure. In contrast, areas exhibiting minimal deformation, including zones of slight uplift, are predominantly located in the northwest and southwest sectors of the airport, which correspond to built-up zones such as terminal complexes and administrative buildings, potentially built on piles extending beyond the soft subsurface sediments to the bedrock.

https://doi.org/10.5194/egusphere-2026-1929
Preprint. Discussion started: 28 April 2026

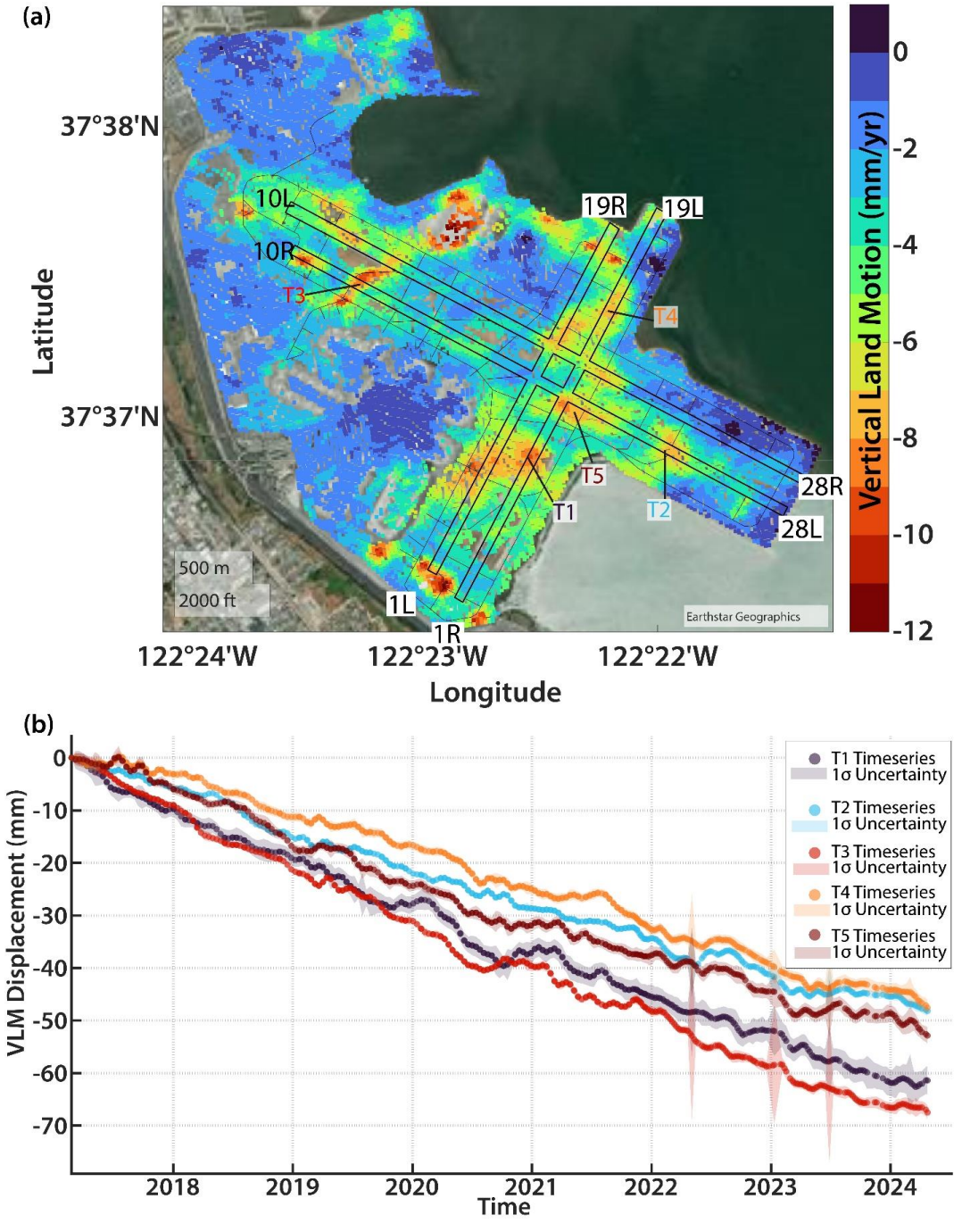

Figure 1. (a) VLM at SFO derived from Sentinel-1 InSAR observations spanning 2017–2024. The color scale represents vertical velocity in mm/year, with positive values indicating uplift and

https://doi.org/10.5194/egusphere-2026-1929
Preprint. Discussion started: 28 April 2026

negative values indicating subsidence. Major runways (10L/28R, 10R/28L, 1L/19R, and 1R/19L) are overlaid for reference. Subsidence hotspots are labelled T1, T2, T3, T4 and T5. (b) VLM time series from 2017 to 2024 at the labelled subsidence hotspots. The chart illustrates vertical displacement in millimeters (mm) derived from InSAR observations at all five locations referenced to the first observation epoch in the IGS14 terrestrial reference frame. Each colored line represents an individual hotspot time series, with associated 1σ uncertainty shaded. Background satellite imagery © Esri, Earthstar Geographics.

3.2 VLM time series at subsidence hotspots

Figure 1b illustrates VLM time series derived from five representative subsidence hotspots within SFO, based on multi-temporal InSAR analysis. The displacement is referenced to the first observation epoch in the IGS14 terrestrial reference frame and spans the period from early 2017 to 2024. Vertical deformation is expressed in millimeters (mm), and the 1σ uncertainty envelopes are shown as shaded regions around each time series.

Each trajectory reflects localized ground motion behavior, with sub-linear subsidence rates ranging from −5.4 mm/year to −8.2 mm/year. While all five sites exhibit long-term downward trends indicative of sustained ground compaction, they also reveal pronounced temporal variability superimposed on the linear trajectories. This includes short-term accelerations, periods of relative stability, and intermittent uplift, likely governed by seasonal fluctuations in groundwater levels, hydromechanical responses of fill material, or episodic anthropogenic activity.

T3 (red dashed line) demonstrates the most rapid and persistent subsidence, with a linear velocity of −9.1 ± 0.1 mm/year. The nearly monotonic pattern, with limited seasonal modulation, suggests dominance of long-term consolidation processes, potentially associated with thick layers of hydraulically placed fill over compressible Bay Mud. T1 and T5 display similar subsidence rates of −8.4 ± 0.1 mm/year and −6.9 ± 0.1 mm/year, respectively. These sites exhibit moderate seasonal variability, potentially driven by cyclic groundwater recharge and discharge, or surface loading effects associated with adjacent infrastructure. T2 and T4 show comparatively slower subsidence rates of −6.5 ± 0.04 mm/year and −6.4 ± 0.04 mm/year, respectively. Both time series present evidence of episodic accelerations and decelerations in deformation, which may reflect interactions between hydroclimatic factors, construction activity, and spatially variable geotechnical properties of the subsurface.

The persistence of predominantly linear subsidence across all sites supports the hypothesis of ongoing secondary consolidation within the underlying unconsolidated deposits. However, the intermittent non-linearities, particularly the brief reversals or plateaus observed in early 2021,

https://doi.org/10.5194/egusphere-2026-1929
Preprint. Discussion started: 28 April 2026

highlight the influence of transient deformation mechanisms. These may include regional seismic activity, rapid changes in hydraulic head or load changes.

3.3 Cross-sectional Analysis of Vertical Displacement and Subsurface Stratigraphy at SFO

Figure 2 presents an integrated cross-sectional view of vertical ground displacement and subsurface stratigraphy along a 3.2-km transect (A–A′) across SFO. The figure is divided into three panels: Panel A illustrates the extent of reclaimed land at SFO by construction year (1943, 1956, 1968, and 1974) and its paleoenvironmental settings, including tidal marsh, tidal flat, shell flat, island, and shallow bay. It also shows the ~~geotechnic~~ data points and the cross-sectional profile AA′. Panel B illustrates cumulative vertical displacement from 2017 to 2024, while the lower panel depicts a detailed subsurface geologic cross-section, revealing the vertical and lateral heterogeneity of subsurface materials. The displacement is expressed in centimeters and temporally color-coded, showing a pattern of progressive subsidence with subtle annual fluctuations likely driven by seasonal groundwater dynamics. Several pronounced subsidence troughs are observed at approximately 0.2 km, 1.7 km, and 2.3 km along the profile, indicating localized zones of enhanced consolidation. Historical shoreline boundaries from 1943, 1956, and 1968 are superimposed, corresponding to key phases of land reclamation and providing essential context for anthropogenic modifications of the landscape. The paleoenvironmental zones, tidal marsh, tidal flat, shallow bay, and shell flat, further highlight the site's transitional coastal origin, characterized by soft, water-saturated sediments that now underlie engineered fill.

The lower panel presents a high-resolution geologic cross-section delineating five primary stratigraphic units: artificial fill, young bay mud, Holocene alluvium, old bay mud, and Pleistocene alluvium. This profile reflects a complex Quaternary depositional history characterized by alternating layers of highly compressible fine-grained sediments and more competent granular materials, including discrete coarse-grained lenses. The heterogeneous subsurface architecture exerts a primary control on the spatial variability of differential subsidence observed along the 3.2 km transect. Variations in the thickness of the young bay mud, ranging from approximately 5 to 70 feet (1.5 to 21 meters), are particularly influential, with the most pronounced subsidence occurring between 0–0.5 km and 1.5–2.5 km, where these deposits are thickest. In contrast, zones of relative surface stability or slight uplift align with areas underlain by shallower alluvium materials. Although a strong spatial correlation exists between the young bay mud thickness and the vertical deformation, the location of the maximum deformation (0.2 km along profile) does not coincide with the greatest thickness of young bay mud, suggesting additional controls such as paleoenvironmental conditions, the chronology of land reclamation, and the method of fill emplacement. The artificial fill layer, which is generally thicker over in later reclamation years and thinner in earlier years, reflects varying reclamation strategies employed over time. These differences in fill placement, along with associated variations in preloading, drainage conditions, and consolidation behavior, likely contribute to the non-uniform deformation response.

https://doi.org/10.5194/egusphere-2026-1929
Preprint. Discussion started: 28 April 2026

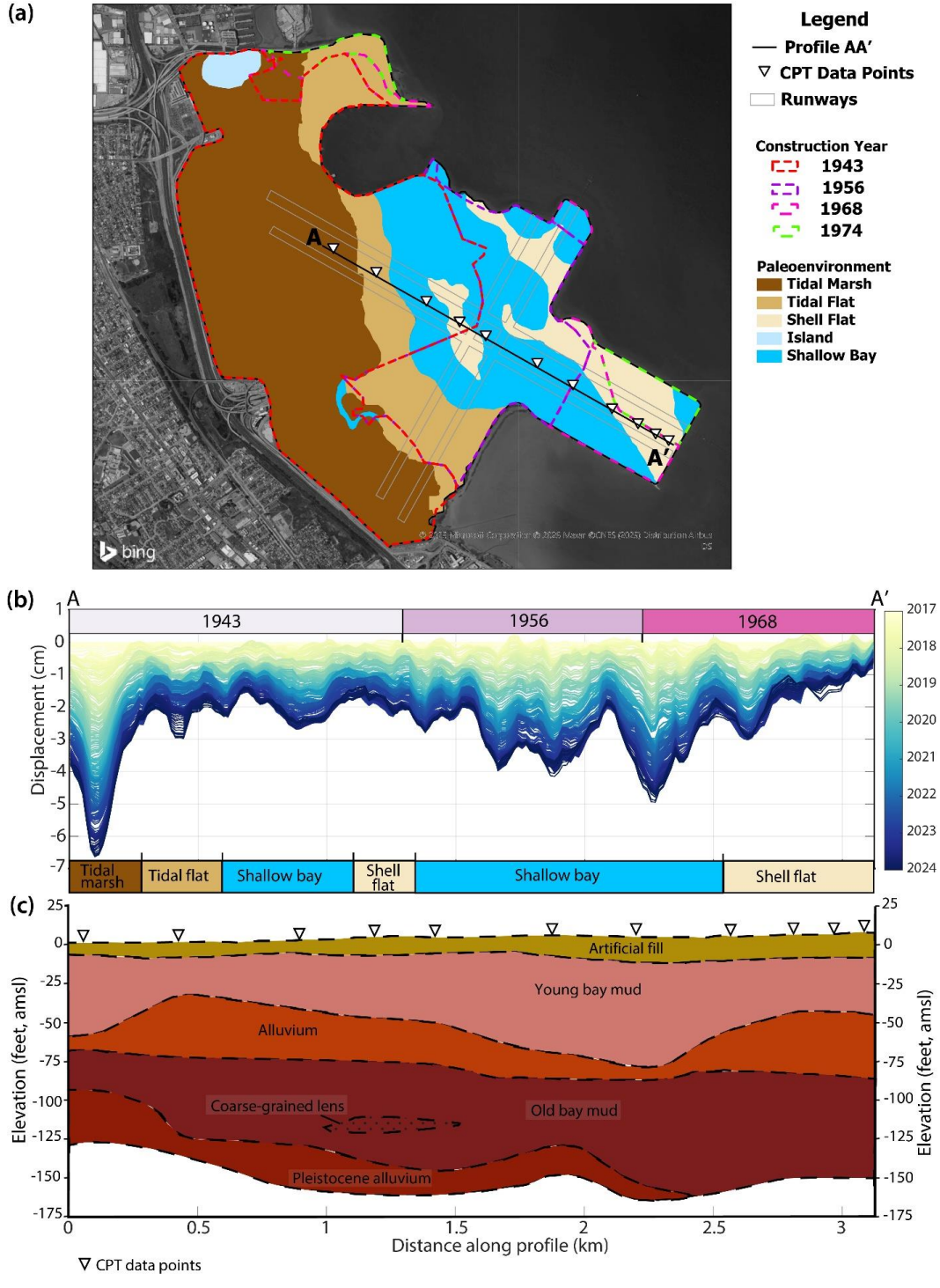

264

https://doi.org/10.5194/egusphere-2026-1929
Preprint. Discussion started: 28 April 2026

Figure 2. Cross-sectional subsidence and stratigraphy along a 3.2 km transect (A–A′) at SFO. **Panel A** illustrates the extent of reclaimed land at SFO by completed construction year (1943, 1956, 1968, and 1974) and its paleoenvironmental settings including tidal marsh, tidal flat, shell flat, island, and shallow bay (modified from (Fugro, 2013)). **Panel B** depicts cumulative vertical displacement along transect AA' from 2017 to 2024, revealing differential subsidence patterns associated with construction history and underlying paleoenvironmental conditions. **Panel C** presents the subsurface stratigraphy derived from the geotechnic investigation (modified from (Fugro, 2013)), highlighting distinct geological layers such as artificial fill, Young Bay Mud, alluvium, Old Bay Mud with coarse-grained lenses, and Pleistocene alluvium. This integrated profile emphasizes the relationship between historical reclamation practices, subsurface geology, and observed vertical land motion. Background satellite imagery © Microsoft Corporation, provided via Bing Maps; imagery content © 2025 Maxar, © CNES, Distribution Airbus.

3.4 Other Possible Land Subsidence Drivers at SFO

Analysis of VLM across all four runways at SFO reveals that deformation rates vary systematically with both construction history and paleoenvironmental conditions (Fig. 3a). Sites constructed during earlier reclamation phases (1943, 1956, and 1968) exhibit significantly greater subsidence rates, with vertical displacements reaching up to −6 to −9 mm/year. In contrast, areas constructed in 1974 show minimal deformation, suggesting that improvements in ground preparation and fill compaction practices reduced subsequent settlement. The underlying paleoenvironment also plays a critical role: regions built over Tidal Marsh and Shallow Bay deposits experience greater settlement, reflecting the compressibility of underlying soft clays and silts, whereas areas over Shell Flat and Tidal Flat environments exhibit reduced settlement associated with firmer, less compressible soils.

Comparison of VLM between touchdown and non-touchdown zones across all four runways (Fig. 3b) indicates a statistically significant difference (t-statistic = −4.03, p-value ≈ 0.00005). However, the magnitude of this difference is modest when compared to the more pronounced impacts of construction history and paleoenvironmental conditions. Additionally, the observed touchdown zones may not uniformly experience consistent aircraft landing loads, potentially further reducing the detected effect. Consequently, while repetitive aircraft loading does contribute to localized differential settlement, it remains a secondary factor relative to broader geotechnical and historical influences.

The results of the geographical (factor) detector analysis (Fig. 3c) quantitatively reinforce these observations. Among the three variables considered, construction year explains the largest share of VLM variance (18.6%), highlighting the long-term influence of historical fill practices. Paleoenvironment accounts for 14.3% of the variance, affirming the strong control exerted by

https://doi.org/10.5194/egusphere-2026-1929
Preprint. Discussion started: 28 April 2026

natural geological conditions. Touchdown zone effects account for only 0.7% of the variance, underscoring that operational loading, while statistically detectable, plays a comparatively minor role in driving settlement along runways. In total, construction year, paleoenvironment and touchdown zone account for less than 35% of the variance in the VLM dataset along runways.

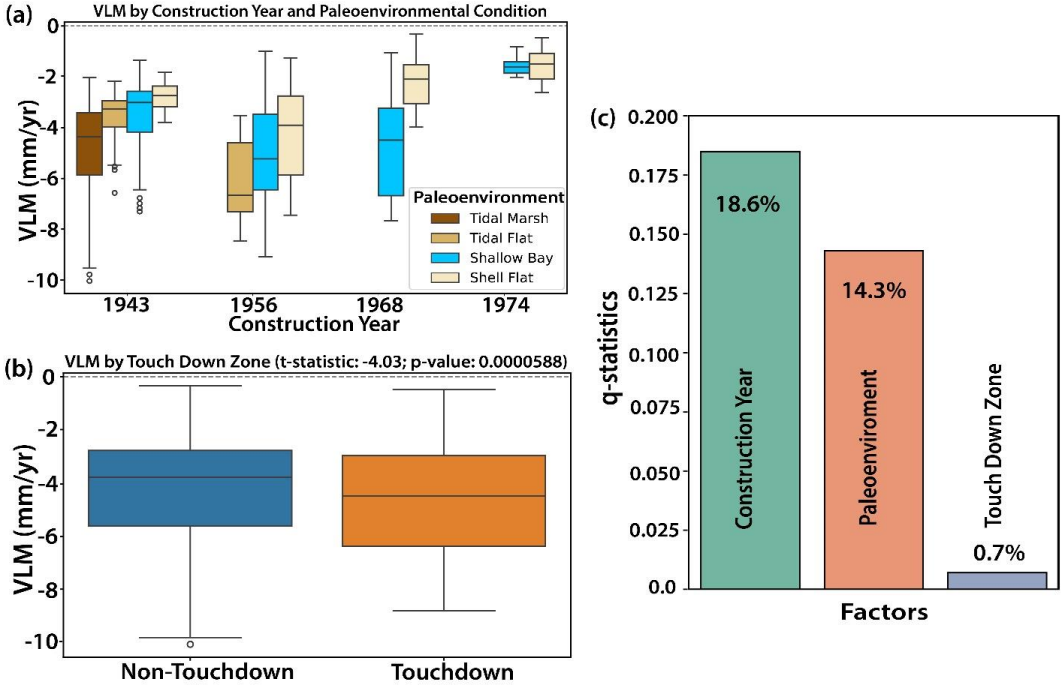

Figure 3. Influence of construction history, paleoenvironmental setting, and infrastructure usage on VLM along runways at SFO. (a) Boxplots of VLM rates (mm/year) grouped by construction year (1943, 1956, 1968, and 1974) and paleoenvironmental condition (Tidal Marsh, Tidal Flat, Shallow Bay, Shell Flat). Results show that earlier construction phases and specific paleoenvironmental settings (e.g., Tidal Marsh) are associated with higher subsidence rates, while later construction (1974) exhibits relatively stable conditions. (b) Comparison of VLM between touchdown zones (areas subjected to frequent aircraft landing impacts) and non-touchdown areas. Touchdown zones show statistically higher subsidence rates, as indicated by a significant t-test result (t-statistic = −4.03, p-value < 0.0001). (c) Bar plot of q-statistics from a geographical detector analysis, quantifying the variance in VLM explained by each factor. Construction year accounts for 18.6% of the variance, paleoenvironmental condition for 14.3%, and touchdown zone presence for 0.7%, highlighting construction history as the dominant driver of observed VLM patterns.

https://doi.org/10.5194/egusphere-2026-1929
Preprint. Discussion started: 28 April 2026

3.5 Runway Displacement Profiles

Figure 4 illustrates the progressive vertical displacement along the four runways (1L/19R, 1R/19L, 10L/28R, and 10R/28L) at SFO between 2017 and 2024. Several important patterns emerge across all runways, displacement profiles generally deepen year after year, as indicated by the gradual shift from lighter (2017) to darker (2024) colors. This reflects a clear temporal trend of ongoing vertical settlement, with cumulative displacements reaching several centimeters over the observation period. Rather than uniform displacement along each runway, multiple localized subsidence "troughs" appear, especially pronounced at specific distances. These troughs likely correspond to underlying variations in subsurface composition, such as differences between fill, soft bay mud, or paleoenvironment, and varying mechanical properties along the runways.

Runways 10L/28R and 10R/28L (the east-west runways) exhibit larger and more complex patterns of subsidence compared to 1L/19R and 1R/19L. These differences may reflect heavier aircraft traffic (including frequent landings of larger jets) and greater cumulative stresses. Particularly along 10R/28L, deeper subsidence troughs are visible near the touchdown zones (2-3 km), where repeated mechanical loading likely exacerbates consolidation of underlying materials.

The narrowing vertical separation between successive annual deformation profiles toward the end of the observation period (2022–2024) indicates a deceleration of subsidence in several sections of the runways. Given the historical sequence of land reclamation and the underlying geotechnical context at SFO, this trend is most consistent with secondary consolidation (creep) and reduction in soil permeability, both time-dependent processes that produce diminishing settlement rates once excess pore pressures have fully dissipated (Jian et al., 2012; Kooi and Erkens, 2020; Liu et al., 2020; Wang et al., 2021). Nonetheless, the localized differential settlement along the runways presents potential hazards, including pavement cracking, surface irregularities, and compromised operational safety margins. If these patterns continue, maintenance interventions (e.g., resurfacing, subsurface ground improvement) will be necessary to preserve safe operating conditions and limit disruptions.

https://doi.org/10.5194/egusphere-2026-1929
Preprint. Discussion started: 28 April 2026

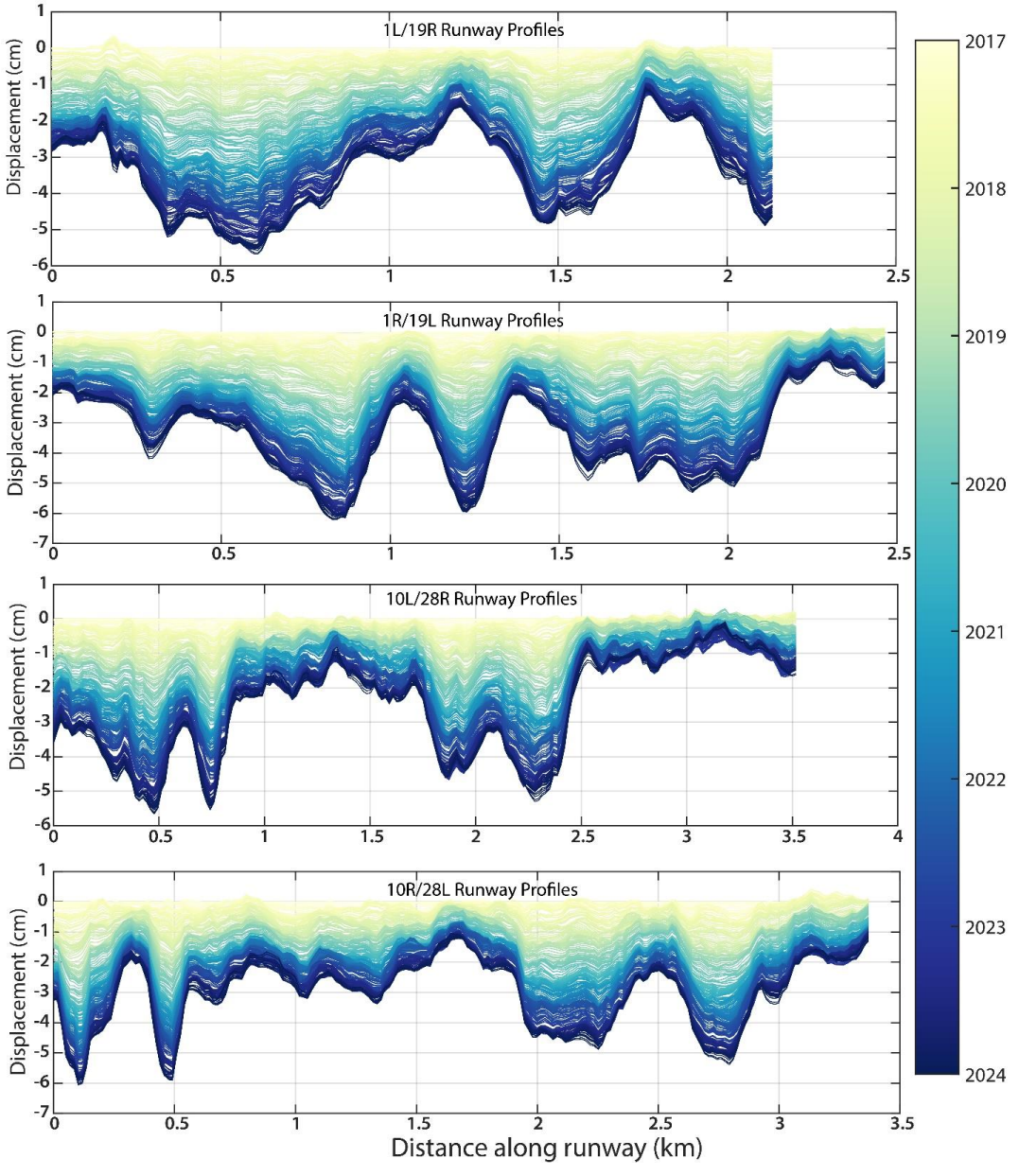

346

347 **Figure 4. Time-evolving surface displacement profiles along major runways at San Francisco**
348 **International Airport (SFO).** Each subplot shows sequential displacement profiles along the
349 length of four primary runways, 1L/19R, 1R/19L, 10L/28R, and 10R/28L, from 2017 to 2024. The
350 y-axis indicates cumulative vertical displacement in centimeters, while the x-axis represents
351 distance along each runway (in kilometers). Line color transitions from light yellow (earlier years)

https://doi.org/10.5194/egusphere-2026-1929
Preprint. Discussion started: 28 April 2026

to dark blue (later years) according to the color scale bar, capturing progressive subsidence patterns over time. Distinct subsidence troughs, spatially localized along runway segments, are evident, indicating differential settlement likely associated with variations in underlying fill materials, usage intensity, and construction history.

4 Discussion

This study presents a detailed assessment of VLM spatiotemporal distribution and drivers across SFO based on spatially continuous InSAR observations and integrated geotechnical data. The analysis reveals that subsidence patterns are controlled by a complex interplay of historical land reclamation practices, paleoenvironmental setting, subsurface stratigraphy, and, to a lesser extent, operational aircraft loading. The spatial variability in subsidence rates at SFO closely aligns with the thickness of the underlying Young Bay Mud deposits, while fill emplacement techniques, natural paleoenvironmental settings and construction chronology may have secondary influence. This observation has significant implications for infrastructure performance, operational safety, and long-term resilience in a changing coastal environment.

Spatially heterogeneous subsidence generates differential vertical displacement across pavement structures, imposing bending stresses that rigid concrete pavements are particularly ill-suited to accommodate. Where displacement gradients approach several millimeters per year across distances of tens to hundreds of meters, as observed at runway intersections and subsidence troughs at SFO, these stresses promote fatigue cracking, joint faulting, and slab rocking in rigid pavements, and rutting and longitudinal cracking in flexible systems (Fig. 5) (Cigna et al., 2012; Dasho and Shirzaei, 2025; Ohenhen et al., 2024). Localized surface depressions formed by differential settlement create persistent ponding zones that reduce skid resistance, accelerate subgrade saturation, and impair stormwater drainage efficiency (Dasho and Shirzaei, 2025). Cumulatively, these deformation-induced defects reduce pavement service life, escalate maintenance expenditure, and introduce operational safety risks for aircraft during ground movement phases where surface continuity tolerances are tightly regulated by aviation authorities.

Beyond localized pavement distress, subsidence fundamentally alters SFO's exposure to coastal flooding by amplifying effective RSLR at the airfield surface. The subsidence rates of -5 to -8 mm/yr documented here add directly to projected regional SLR of 0.19 m by 2100 under SSP 2-4.5 (Garner et al., 2021). Expressed cumulatively, subsidence alone, projected linearly and therefore likely representing an upper bound given the deceleration observed in recent years, could lower airfield surface elevations by 0.38–0.60 m by 2100, a magnitude larger than the projected regional SLR under low-to-intermediate emissions scenarios over the same period. This compounding effect accelerates the timeline to critical thresholds, including recurrent tidal inundation under fair-weather conditions, progressive loss of freeboard in shoreline protection

https://doi.org/10.5194/egusphere-2026-1929
Preprint. Discussion started: 28 April 2026

structures, increased storm surge penetration, and declining surface elevation relative to fixed stormwater drainage infrastructure. Runways 10R/28L and 10L/28R, underlain by the thickest compressible deposits, face the earliest onset of these compounding hazards.

Given these converging challenges, adaptive maintenance and resilience planning at SFO must integrate both differential subsidence and RSLR projections into engineering design standards, risk assessment frameworks, and long-term capital improvement plans. Potential strategies include continuous monitoring of ground deformation using multi-sensor InSAR; targeted ground improvement (e.g., deep soil mixing, stone columns) beneath critical infrastructure to arrest or slow secondary consolidation; strengthening flood defenses; upgrading stormwater management systems to accommodate accelerated relative sea-level rise; and integrating flexible pavement designs that can tolerate differential movement. Ultimately, effective resilience strategies will require a combined approach addressing both the geotechnical realities of ongoing land deformation and the climate-driven threats of sea-level rise. SFO's experience can serve as a critical case study for other major airports and coastal infrastructure hubs worldwide that are increasingly challenged by the intersection of anthropogenic subsidence and extreme weather event.

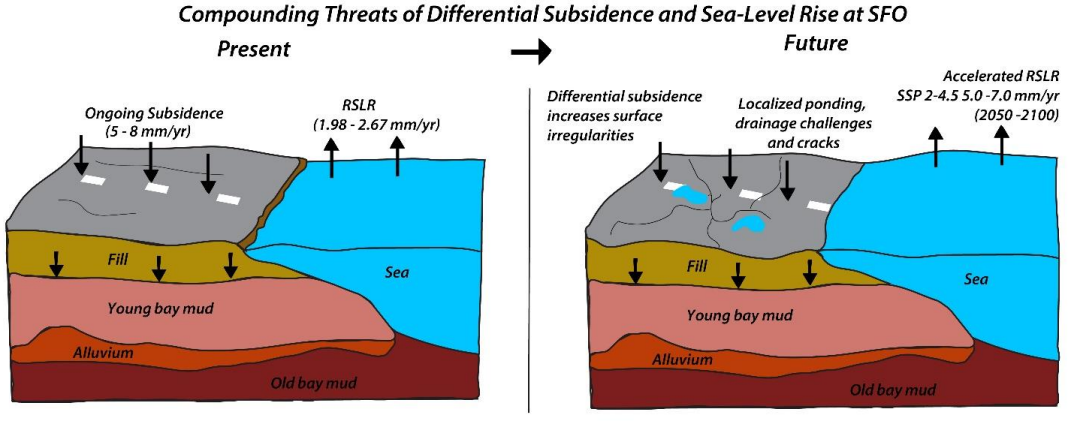

Figure 5. Structural and Hydrological Impacts of Progressive Subsidence at SFO: Illustration showing how ongoing land subsidence SFO could cause surface cracking, runway deformation, water ponding and elevation loss, which compromise shoreline protection and increase exposure to coastal flooding under rising sea level.

Conclusion

This study provides a spatially dense assessment of VLM across SFO, revealing that ongoing ground deformation is predominantly governed by the complex interplay between historical land

https://doi.org/10.5194/egusphere-2026-1929
Preprint. Discussion started: 28 April 2026

reclamation practices, underlying subsurface stratigraphy, and, to a lesser extent, operational aircraft loading. Subsidence is most pronounced where thick, compressible Young Bay Mud deposits underlie hydraulically placed fill, with localized rates exceeding −10 mm/year.

Temporal analysis indicates a general deceleration of subsidence in recent years, nevertheless, localized differential settlement persists, posing operational risks such as pavement distress, surface ponding, and reduced structural serviceability. These effects, compounded by subsidence-driven amplification of relative sea-level rise rates, threaten to accelerate the loss of functional freeboard for SFO's coastal protection systems and increase the likelihood of tidal and storm-induced flooding.

Given these challenges, continuous deformation monitoring, integration of ground improvement technologies, elevation enhancement of critical infrastructure, and updated drainage designs must be incorporated into SFO's long-term resilience planning. More broadly, the insights gained from SFO underscore the urgent need for integrated geotechnical and climate adaptation strategies at coastal airports worldwide, where the intersection of anthropogenic subsidence and climate change represents an emerging threat to critical transportation infrastructure.

Code and Dataset Availability

The Sentinel-1 dataset used in this study can be accessed through the Alsaka Satetllite Facility at https://asf.alaska.edu/. The GNSS dataset can be accessed through Nevada Geodetic Laboratory at https://geodesy.unr.edu/. The WabInSAR software used for InSAR processing can be accessed via https://www.eoivt.com/software. The VLM dataset (Dasho and Shirzaei, 2026) referenced in this manuscript are publicly available via the Virginia Tech Data Repository at https://doi.org/10.7294/31974768.

Author contribution

OD and MS designed the experiments and OD carried them out. OD prepared the manuscript. MS revised and edited the manuscript.

Competing interests

The authors declare that they have no conflict of interest.

Acknowledgement

This work is supported by the National Academies of Sciences, Engineering and Medicine, Airport Cooperative Research Program (ACRP) Graduate Research Award.

Funding

OD was supported by National Academies of Sciences, Engineering and Medicine, Airport Cooperative Research Program (ACRP) Graduate Research Award. MS is supported by the US Department of Defense.

https://doi.org/10.5194/egusphere-2026-1929
Preprint. Discussion started: 28 April 2026

References

Baldwin, J., Bartow, G. W., Dartnell, P., Ford, G., Gilman, J. A., Gilver, R., and Goodin, S.: Geology of San Francisco, California, Geol. Cities World Ser., 189, 2018.

Bianchini Ciampoli, L., Gagliardi, V., Clementini, C., Latini, D., Del Frate, F., and Benedetto, A.: Transport Infrastructure Monitoring by InSAR and GPR Data Fusion, Surv. Geophys., 41, 371–394, https://doi.org/10.1007/s10712-019-09563-7, 2020.

Blackwell, E., Shirzaei, M., Ojha, C., and Werth, S.: Tracking California's sinking coast from space: Implications for relative sea-level rise, Sci. Adv., 6, 1–10, https://doi.org/10.1126/sciadv.aba4551, 2020.

Chen, B., Gong, H., Chen, Y., Li, X., Zhou, C., Lei, K., Zhu, L., Duan, L., and Zhao, X.: Land subsidence and its relation with groundwater aquifers in Beijing Plain of China., Sci. Total Environ., 735, 139111, https://doi.org/10.1016/j.scitotenv.2020.139111, 2020.

Cigna, F., Osmanoğlu, B., Cabral-Cano, E., Dixon, T. H., Ávila-Olivera, J. A., Garduño-Monroy, V. H., DeMets, C., and Wdowinski, S.: Monitoring land subsidence and its induced geological hazard with Synthetic Aperture Radar Interferometry: A case study in Morelia, Mexico, Remote Sens. Environ., 117, 146–161, https://doi.org/10.1016/j.rse.2011.09.005, 2012.

Costantini, M. and Rosen, P. A.: Generalized phase unwrapping approach for sparse data, in: International Geoscience and Remote Sensing Symposium (IGARSS), 267–269, https://doi.org/10.1109/igarss.1999.773467, 1999.

Dasho, O. and Shirzaei, M.: Sinking Airports: A Glance at the State of US Transport Infrastructure, Earth Space Sci., 12, e2025EA004433, https://doi.org/10.1029/2025EA004433, 2025.

Dasho, O. and Shirzaei, M.: Monitoring Land Subsidence at San Francisco International Airport Using Satellite Radar Interferometry, https://doi.org/10.7294/31974768, 2026.

De Vivo, C., Ellena, M., Capozzi, V., Budillon, G., and Mercogliano, P.: Risk assessment framework for Mediterranean airports: a focus on extreme temperatures and precipitations and sea level rise, Nat. Hazards, 111, 547–566, https://doi.org/10.1007/s11069-021-05066-0, 2022.

Farr, T. G., Rosen, P. A., Caro, E., Crippen, R., Duren, R., Hensley, S., Kobrick, M., Paller, M., Rodriguez, E., Roth, L., Seal, D., Shaffer, S., Shimada, J., Umland, J., Werner, M., Oskin, M., Burbank, D., and Alsdorf, D. E.: The shuttle radar topography mission, Rev. Geophys., 45, 1–13, 2007.

Franceschetti, G. and Lanari, R.: Synthetic aperture radar processing CRC press, Electron. Eng. Syst. Ser., 1999.

Fugro: Preliminary Assessment of Earthquake-Induced Liquefaction Susceptibility at Five San Francisco Bay Area Airports, 2013.

Gagliardi, V., Bianchini Ciampoli, L., Trevisani, S., D'amico, F., Alani, A. M., Benedetto, A., and Tosti, F.: Testing sentinel-1 sar interferometry data for airport runway monitoring: A geostatistical analysis, Sensors, 21, https://doi.org/10.3390/s21175769, 2021.

https://doi.org/10.5194/egusphere-2026-1929
Preprint. Discussion started: 28 April 2026

Garner, G. G. et al.: IPCC AR6 Sea-Level Rise Projections. https://podaac.jpl.nasa.gov/announcements/2021-08-09-Sea-level-projections-from-the-IPCC-6th-Assessment Report ., 2021.

Govorcin, M., Bekaert, D. P. S., Hamlington, B. D., Sangha, S. S., and Sweet, W.: Variable vertical land motion and its impacts on sea level rise projections, Sci. Adv., 11, https://doi.org/10.1126/sciadv.ads8163, 2025.

Griggs, G.: Coastal Airports and Rising Sea Levels, J. Coast. Res., 36, 1079, https://doi.org/10.2112/JCOASTRES-D-20A-00004.1, 2020.

Hanssen, R. F.: Radar Interferometry: Data Interpretation and Error Analysis - Ramon F. Hanssen - Google Books, Springer, 2001.

Jian, W., Chongyang, S., Hui, I., Shaoan, S., and Lelin, X.: Gravity inversion of deep-crust and mantle interfaces in the Three Gorges area, Geod. Geodyn., 3, 7–17, https://doi.org/10.3724/sp.j.1246.2012.0008, 2012.

Johnson, A., Trivedi, D., Hanegan, K., and Yu, R.: PROTECTING THE SHORELINE OF THE SAN FRANCISCO INTERNATIONAL AIRPORT FROM SEA LEVEL RISE, Coast. Eng. Proc., 42, https://doi.org/10.9753/icce.v36.risk.42, 2018.

Kooi, H. and Erkens, G.: Creep consolidation in land subsidence modelling; integrating geotechnical and hydrological approaches in a new MODFLOW package (SUB-CR), in: Proceedings of IAHS, TISOLS: the Tenth International Symposium on Land Subsidence; living with subsidence - Tenth International Symposium on Land Subsidence, Delft, the Netherlands, 17–21 May 2021, 499–503, https://doi.org/10.5194/piahs-382-499-2020, 2020.

Lee, J. C. and Shirzaei, M.: Novel algorithms for pair and pixel selection and atmospheric error correction in multitemporal InSAR, Remote Sens. Environ., 286, 113447, https://doi.org/10.1016/j.rse.2022.113447, 2023.

Liu, Y., Li, J., Fang, Z. N., Rashvand, M., and Griffin, T.: The Secondary Consolidation (Creep) due to Geohistorical Overburden Pressure in the Houston-Galveston Region, Texas, in: Proceedings of IAHS, TISOLS: the Tenth International Symposium on Land Subsidence; living with subsidence - Tenth International Symposium on Land Subsidence, Delft, the Netherlands, 17–21 May 2021, 315–320, https://doi.org/10.5194/piahs-382-315-2020, 2020.

Mario Costantini, T.: A novel phase unwrapping method based on network programming, IEEE Trans. Geosci. Remote Sens., 36, 813–821, https://doi.org/10.1109/36.673674, 1998.

Miller, M. M. and Shirzaei, M.: Land subsidence in Houston correlated with flooding from Hurricane Harvey, Remote Sens. Environ., 225, 368–378, https://doi.org/10.1016/j.rse.2019.03.022, 2019.

Moffatt and & Nichol: Colma Creek/ San Bruno Creek Resiliency Study. Prepared for the San Francisco International Airport and the California Coastal Conservancy, 2015.

Nicholls, R. J., Lincke, D., Hinkel, J., Brown, S., Vafeidis, A. T., Meyssignac, B., Hanson, S. E., Merkens, J. L., and Fang, J.: Author Correction: A global analysis of subsidence, relative sea-level change and coastal

https://doi.org/10.5194/egusphere-2026-1929
Preprint. Discussion started: 28 April 2026

518 flood exposure (Nature Climate Change, (2021), 11, 4, (338-342), 10.1038/s41558-021-00993-z), Nat.
519 Clim. Change, 11, 634, https://doi.org/10.1038/s41558-021-01064-z, 2021.

520 Ohenhen, L. O., Shirzaei, M., and Barnard, P. L.: Slowly but surely: Exposure of communities and
521 infrastructure to subsidence on the US east coast, PNAS Nexus, 3,
522 https://doi.org/10.1093/pnasnexus/pgad426, 2024.

523 Shirzaei, M.: A wavelet-based multitemporal DInSAR algorithm for monitoring ground surface motion,
524 IEEE Geosci. Remote Sens. Lett., 10, 456–460, https://doi.org/10.1109/LGRS.2012.2208935, 2013.

525 Shirzaei, M. and Bürgmann, R.: Topography correlated atmospheric delay correction in radar
526 interferometry using wavelet transforms, Geophys. Res. Lett., 39, 1–6,
527 https://doi.org/10.1029/2011GL049971, 2012.

528 Shirzaei, M., Freymueller, J., Törnqvist, T. E., Galloway, D. L., Dura, T., and Minderhoud, P. S. J.:
529 Measuring, modelling and projecting coastal land subsidence, Nat. Rev. Earth Environ., 2, 40–58,
530 https://doi.org/10.1038/s43017-020-00115-x, 2020.

531 Stock, S., Nious, K., Carroll, J., and Horn, M.: Sinking, Pooling, Cracking: Runway Problems at San
532 Francisco International Airport Cause More Delays for Travelers, NBC Bay Area, 18th February, 2019.

533 Wang, F., Pang, W., Li, Z., Wei, H., and Han, L.: Experimental Study on Consolidation-Creep Behavior of
534 Subgrade Modified Soil in Seasonally Frozen Areas, Materials, 14, 5138,
535 https://doi.org/10.3390/ma14185138, 2021.

536 Yesudian, A. N. and Dawson, R. J.: Global analysis of sea level rise risk to airports, Clim. Risk Manag., 31,
537 100266, https://doi.org/10.1016/j.crm.2020.100266, 2021.

538 Zhang, Z., Song, Y., and Wu, P.: Robust geographical detector, Int. J. Appl. Earth Obs. Geoinformation,
539 109, 102782, https://doi.org/10.1016/j.jag.2022.102782, 2022.

540